Original Article

Ability of three-dimensional 3-Tesla ultrashort echo time magnetic resonance imaging to display the morphological characteristics of pulmonary nodules: a sensitivity analysis

Funan Wang, Xi Lin, Chong Lin, Guoqiang Huang, Min Li, Liuhong Zhu

Department of Radiology, Xiamen Branch, Zhongshan Hospital, Fudan University, Xiamen, China

Contributions: (I) Conception and design: F Wang, X Lin; (II) Administrative support: C Lin; (III) Provision of study materials or patients: X Lin, C Lin; (IV) Collection and assembly of data: F Wang, X Lin, C Lin; (V) Data analysis and interpretation: C Lin, G Huang, M Li; (VI) Manuscript writing: All authors; (VII) Final approval of manuscript: All authors.

Correspondence to: Liuhong Zhu. Department of Radiology, Xiamen Branch, Zhongshan Hospital, Fudan University, No. 668 of Jinhu Road, Huli District, Xiamen 361015, China. Email: zhuliuhong@163.com.

Background: Radiation-free lung cancer screening will reduce/eliminate radiation exposure in the diagnosis and follow-up of patients with lung cancer.

Methods: This was a prospective study. The participants were recruited using convenience sampling. A total of 36 patients with pulmonary nodules [patients with single or multiple pulmonary nodules >4 and <30 mm on their pulmonary computed tomography (CT) scans] who were admitted to Fudan University Zhongshan Hospital's Xiamen branch were enrolled; they underwent a CT scan and a free-breathing ultrashort time-of-echo (UTE) sequence scan using a 3-Tesla (T) magnetic resonance imaging (MRI) scanner. The CT examinations were regarded as the reference standard. Patients had an interval time of <3 days between their CT and MRI examinations. Two reviewers with more than 10 years' experience in the diagnosis of pulmonary nodules identified the numbers and morphological features of the pulmonary nodules.

Results: Among the 36 patients, 46 nodules were detected on CT images, 45 of which were also detected on UTE images (a detection rate of 97.6%). The detection rate for lobulation using UTE–MRI was 96.9%; however, the difference compared with the rate for the CT images was not statistically significant (P>0.05). In terms of confounding lesions (confounding lesions indicate that the patient has malignant tumours, benign nodules or inoperable nodules), the UTE–MRI method had a higher detection rate than the CT method, and the difference was significant (P<0.05). The probability of malignant lesions was found to be higher in confounding lesions than in homogeneous lesions. In terms of pleural traction, the UTE–MRI method demonstrated a higher detection rate (120%) than the CT method, but the difference was not statistically significant (P>0.05). In terms of spiculation, the UTE–MRI method demonstrated a lower detection rate (81.8%) than the CT method, although the difference was not statistically significant (P>0.05).

Conclusions: Overall, 3-T UTE–MRI imaging has a high detection rate for pulmonary nodules >4 mm and is similar to that of conventional CT imaging. The method can be used for radiation-free lung cancer screening and follow-up examinations to reduce/eliminate both repeat CT examinations and radiation damage.

Keywords: Ultrashort echo time; morphological characteristics; lungs; pulmonary nodules; magnetic resonance imaging (MRI)

Submitted Feb 08, 2022. Accepted for publication Nov 21, 2022. Published online Jan 02, 2023.
doi: 10.21037/qims-22-118
View this article at: https://dx.doi.org/10.21037/qims-22-118

Introduction

Lung cancer is the most commonly diagnosed cancer and the leading cause of cancer death (1). In USA, the National Lung Screening Trial demonstrated that screening high-risk patients with low-dose computed tomography (CT) of the chest reduces lung cancer mortality compared with screening with chest X-rays (2). The accurate segmentation of the pulmonary nodules on CT scans plays a crucial role in the evaluation and management of patients with suspected lung cancer (3). However, low-dose CT emits radiation, and the probability of carcinogenesis-induced lung cancer is around 0.5–5.5% higher in patients undergoing long-term low-dose CT than in those not undergoing CT scanning (4). Radiation-free lung cancer screening will reduce/eliminate the use of radiation exposure in the diagnosis and follow-up of patients with lung cancer.

Magnetic resonance imaging (MRI) has the clear advantages of high soft-tissue resolution and no radiation. However, characteristics such as low proton density and quick transverse relaxation time (T2) signal attenuation restrict the use of this technique for the lungs, limiting its therapeutic utility. With the advancement of the associated technology, many academics have used MRI examinations to investigate image quality and diagnose pulmonary-related disorders, especially in terms of sequence scanning (5). Specifically, the ultrashort time-of-echo (UTE) technique has undergone rapid development. This technique is characterised by a TE that can be reduced to the microsecond level; therefore, it is particularly suitable for the MRI examination of tissue with short T2 components and inhomogeneous magnetic fields (e.g., lung tissue) since the signal is acquired at the early decay stage of the protons' MR signal (6). In previous studies, Burris *et al.* (7) and Ohno *et al.* (8) used the UTE technique to detect small pulmonary nodules, but they did not analyse morphological characteristics. Elsewhere, Wielpütz *et al.* (9) analysed the morphological characteristics of pulmonary nodules in MRI but did not study their internal signal (i.e., the signal in the parenchyma of the nodule), they compared a 3-Tesla (T) UTE–MRI method with conventional CT imaging in terms of the detection of small pulmonary nodules, with the clinical application value of the former assessed by observing solid and part-solid nodules along the nodule margins. Herein, we present the following article in accordance with the STARD reporting checklist (available at https://qims.amegroups.com/article/view/10.21037/qims-22-118/rc).

Methods

Subjects

This was a prospective study. The participants were recruited using convenience sampling. Imaging data were collected from 106 patients who underwent chest CT examinations between May 2019 and May 2020 at Fudan University Zhongshan Hospital's Xiamen branch and were found to have pulmonary nodules. Following this, MRI examinations were performed. All the MRI scans involved the use of an axial UTE sequence. According to the inclusion and exclusion criteria, 36 patients were finally included in the study. Among them, 23 were male and 13 were female, with an age range of 29–70 years and an average age of 59.30±9.86 years. According to previous studies (9-12), in comparison with nodules of other sizes, UTE is more sensitive in detecting nodules >4 mm in diameter; thus, any nodules with a diameter <4 mm were excluded from this study. However, according to clinical experience, most patients' nodules are <30 mm, so to reduce heterogeneity among the patients, any patients with nodules >30 mm were also excluded.

The inclusion criteria were as follows: (I) patients with single or multiple pulmonary nodules >4 and <30 mm on their pulmonary CT scans, (II) patients who were able to cooperate fully with the scanning protocol to complete the scans, with scan images of excellent quality, (III) patients without other underlying diseases, such as emphysema and (IV) patients with a time interval of <3 days between their CT and MRI examinations. The exclusion criteria included patients with images in the 'bad' or 'very bad' categories.

This study was conducted in accordance with the principles of the Declaration of Helsinki (as revised in 2013). All the patients signed an informed consent form prior to the examination, and all examinations were approved by the ethics committee of Fudan University Zhongshan Hospital's Xiamen Branch. This research was initiated by Xiamen Municipal Health Commission and undertaken at Zhongshan Hospital. As no financial support was received from any pharmaceutical enterprise, and no relevant drugs were used during the trial, there was no registration requirement for this study. Furthermore, the study did not have a registered study protocol.

Examination method

Computed tomography examination

A United Imaging uCT® 64-layer spiral CT scanner

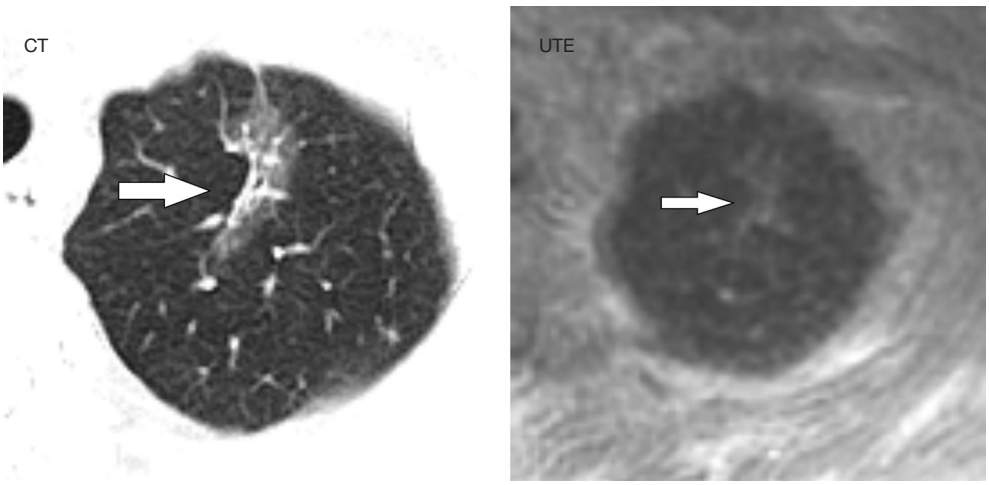

Figure 1 Detection of pulmonary nodules by UTE and CT. The arrow shows the nodule. CT, computed tomography; UTE, ultrashort time of echo.

(Philips, USA) was used. All the patients were encouraged to breathe calmly during scanning and were placed in the supine position, with the feet entering first and both upper limbs raised. The patients were scanned from the lung apex to the lung base under the following parameters: layer thickness =5.0 mm, layer spacing =5.0 mm, pitch =1.375 and tube voltage =120 kV. The automatic tube current technique was used, and 2-mm-thick images were reconstructed. The average irradiation of the CT scan was 3.88 ms, and no contrast was used.

MRI examination

A GE Healthcare HD 750 3.0-T MR scanner (Waukesha, USA) was used. The patients were positioned in the supine position with their feet entering first; a body surface coil was used, and calming regular breathing exercises were performed prior to the scan. The focal area of the pulmonary nodule found in the CT procedure was scanned in the axial position, and the whole lung was scanned in the coronal position using a respiratory-gating double-echo UTE sequence. The scanning parameters were as follows: time of repetition =10 ms, TE =0.032 and 4.4 ms, no contrast, flip angle =9°, field of view =40 cm, slice thickness =2.0 mm, slice interval =1.0 mm, matrix =512×512, scanning slice number =~20 and scanning time =~6 min.

Image interpretation and post-processing

All images were divided into the categories of 'very bad', 'bad', 'good' and 'very good' (10). The 'very bad' category indicated that the image clarity was poor, and the structure of the pulmonary nodules could barely be displayed. The 'bad' category indicated that the image clarity was good, but the nodule structure was not clear and was not easily distinguishable from the surrounding tissue. The 'good' category indicated that the image was clear and the nodule structure was more obvious, and the 'very good' category indicated that the image and the nodule structure were very clear, with the latter easy to distinguish.

Two reviewers with more than 10 years' experience in the diagnosis of pulmonary nodules read the films, performed a double-blind analysis of the MRI, and then, 1 week later, observed and recorded the CT findings separately. In the case of any disagreement in the observations of the sign analysis, the radiologists discussed the results, and the image quality was re-evaluated according to the image quality grading standards. If a consensus was not reached, the image was not used in the next step. Overall, 15 cases were in the 'very bad' category, 55 cases were in the 'bad' category, 24 cases were in the 'good' category, and 12 cases were in the 'very good' category. The patients with 'good' and 'very good' category images were included in the study (36 cases in total), with 70 cases not proceeding to the next step.

The numbers and locations of the detected pulmonary nodules in the UTE–MRI sequencing and the CT images were recorded (*Figure 1*), and the images were observed separately. The main observations included lobulations, spinous protuberances, pleural tractions and internal structures. The number of lesions, lobulations, spinous protuberances and pleural tractions was observed in the lung window, and the intralesional characteristics were

observed in the mediastinal window. All of the MRI image observations were made using the UTE sequence and correctly adjusted window widths.

Definitions

A 'lobulation' (11) occurred when the contours had a plurality of arcuate protrusions and the curved phases were concave cuts that formed a lobulated shape. A 'pleural attachment' (12,13) referred to an inconsistent spinous protuberance at the edge of the nodule exhibited in the lung window. A 'pleural indentation' (14) was a linear shadow between the pulmonary nodule and the pleura that may have been accompanied by triangular or trumpet-shaped projections of the adjacent visceral pleura. Malignant nodules were characterised by their pleural attachments, lobulations and pleural indentations. The confounding lesions indicated that the patient had malignant tumours, benign nodules or inoperable nodules.

Table 1 Detection rate of pulmonary nodules by CT and UTE

Items	n (%)
CT nodules	46
UTE nodules (detection rate)	45 (97.8%)
χ^2 value	0
P value	1

CT, computed tomography; UTE, ultrashort time of echo.

Statistical analysis

All statistical analyses were performed using IBM SPSS 21.0 statistical software. The χ^2 test was used for count data, and McNemar's test (paired χ^2 test) was used for paired data. A value of $P<0.05$ indicated a statistically significant difference.

Results

The number of lesions revealed using the two different methods

A total of 106 patients were selected, with 36 of them meeting the inclusion criteria of this study. All 36 patients completed the study without withdrawal, and there were no adverse events during its course. Among the 36 patients, a total of 46 pulmonary nodules (average diameter =~13 mm) were found via CT, and 45 were found via UTE–MRI; while the CT detection rate was marginally higher, the difference was not statistically significant (n=45, 97.8%, χ^2=0, P=1; see *Table 1*). The nodules were located mainly in the upper lobe, with details of their distribution and locations presented in *Table 2*.

Table 2 Distribution and location of nodules

Segment	CT (n)	UTE (n)
Anterior segment of right upper lobe	6	6
Apex and posterior segment of right upper lobe	5	5
Medial and lateral segments of right middle lobe	5	5
Dorsal segment of right lower lobe	4	4
Inner and posterior basal segments of right lower lobe	2	1
Anterior and outer basal segments of right lower lobe	3	3
Anterior segment of left upper lobe	5	5
Apical posterior segment of left upper lobe	5	5
Lingual segment of left upper lobe	3	3
Dorsal segment of left lower lobe	3	3
Inner and posterior basal segments of left lower lobe	3	3
Anterior and outer basal segments of left lower lobe	2	2

CT, computed tomography; UTE, ultrashort time of echo.

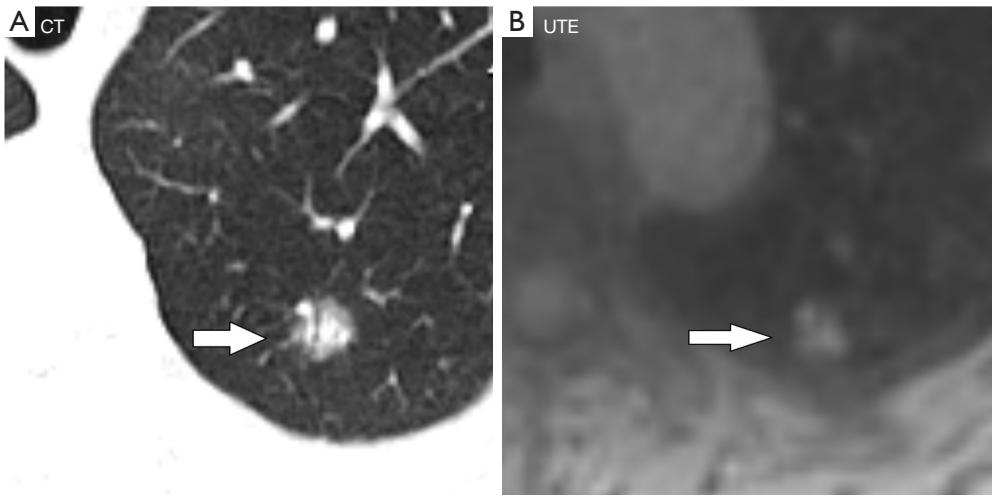

Figure 2 Detection of lobulation by UTE and CT. (A) Left upper lung adenocarcinoma, CT sequences clearly showed the lobulation. (B) Left upper lung adenocarcinoma, UTE sequences clearly showed the lobulation. The arrow shows the lobulation. CT, computed tomography; UTE, ultrashort time of echo.

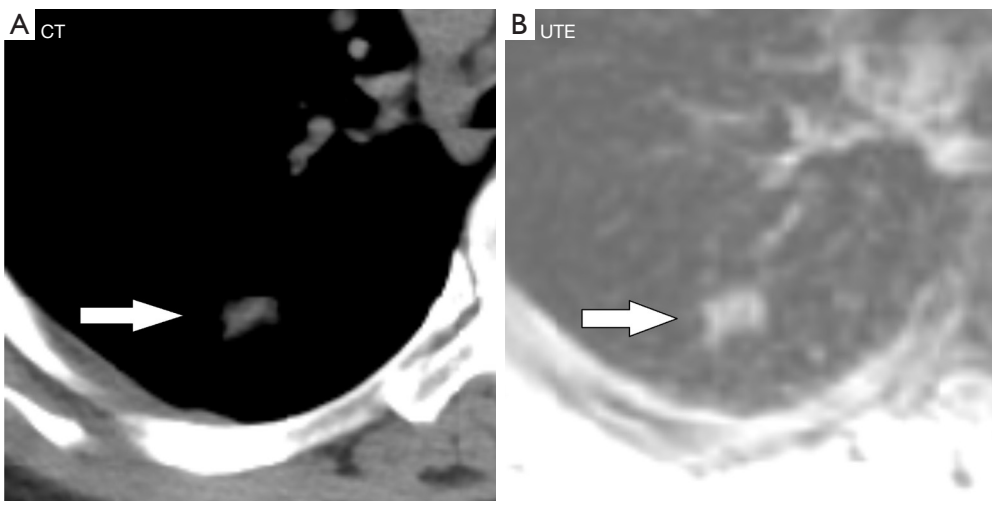

Figure 3 Detection of hypodense shadow and inconsistent high and low signal intensities by UTE and CT. (A) Lung adenocarcinoma in the left upper lobe, CT showed a hypodense shadow in the central solid component of the lesion. (B) Lung adenocarcinoma in the left upper lobe, UTE showed inconsistent high and low signal intensities. The arrow shows hypodense shadow and inconsistent high and low signal intensities. CT, computed tomography; UTE, ultrashort time of echo.

The display of lobulations, spinous protuberances, internal structures and adjacent pleural indentations using the two methods

The UTE–MRI detection rate for lobulation was 97%, similar to that for CT imaging (*Figure 2A*,*2B*), with no significant difference between them. In addition, while the UTE–MRI results suggested different structural signals in the lesions, the CT scans indicated only homogeneous density (*Figure 3A*,*3B*). Lobulations, spinous protuberances, pleural tractions and internal structures were observed, and the results are shown in *Table 3*. The UTE–MRI method demonstrated higher detection rates for heterogeneous changes in the lesions than CT imaging, with significant differences. The number of spinous protuberances revealed by the UTE–MRI images (15) was lower than

Table 3 Number of detected pulmonary nodules by CT and UTE (cases)

Sign	CT (n)	UTE detected (n)	χ^2 value	P value
Lobulation	33	32	0	1
Spinous protuberance	22	18	1.8	0.179
Pleural traction	10	12	0.5	0.480
Structural signals	11	20	7.1	0.007

CT, computed tomography; UTE, ultrashort time of echo.

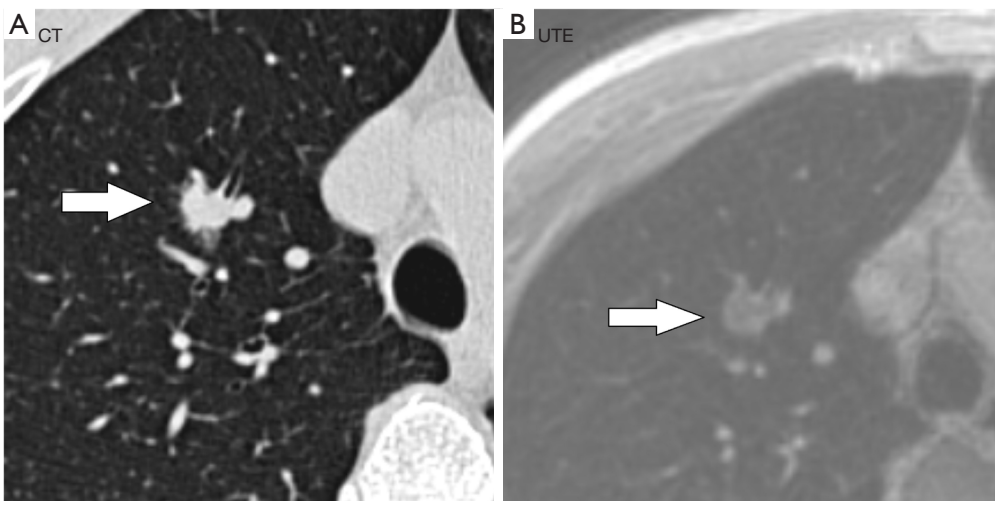

Figure 4 Detection of lesion by UTE and CT. (A) CT sequences of lung adenocarcinoma in the right upper lobe showed spinous protuberance at the edge of the lesion. (B) UTE sequences of lung adenocarcinoma in the right upper lobe showed spinous protuberance at the edge of the lesion. The arrow shows the lesion. CT, computed tomography; UTE, ultrashort time of echo.

that revealed by the CT images (16), but there was no significant difference between the two methods (P>0.05). The UTE–MRI method was less clear in four cases of thin spinous protuberances, while it was similar to CT imaging for 18 thicker spinous protuberances (*Figure 4A*,*4B*). The UTE–MRI technique detected a higher number of pleural indentations (12) than CT imaging (10), but the difference was not statistically significant (P>0.05). Additionally, two UTE–MRI images revealed adjacent subpleural line-like hyperintensity (*Figure 5A*,*5B*) (*Table 2*).

The UTE–MRI images revealed 13 malignant tumours out of 20 confounding lesions, including 12 adenocarcinomas, 1 squamous carcinoma, 5 benign nodules and 2 inoperable nodules. Meanwhile, the CT images revealed 7 malignant tumours out of 11 confounding lesions, including 6 adenocarcinomas, 1 squamous carcinoma, 3 benign nodules and 1 inoperable nodule (*Table 4*).

Discussion

With the maturity and wider use of the technology, the signal-to-noise ratio, tissue contrast, chemical shift resolution and magnetic sensitivity of 3-T MRI images have increased dramatically in recent years. It has been demonstrated that MRI imaging has 100% sensitivity for lung nodules >8 mm in diameter, with a performance comparable to that of CT scanning (17). However, the application of MRI is limited to nodules >8 mm, and its widespread clinical application has not been verified.

Lung tissue contains mainly gas and has an extremely short T2 time and limited signal acquisition. Conventional MR sequence acquisition is not clear, and images of short T2 components may not be acquired. The UTE sequence technique has developed rapidly in recent years and is now mainly used to acquire short T2 components. Its principle

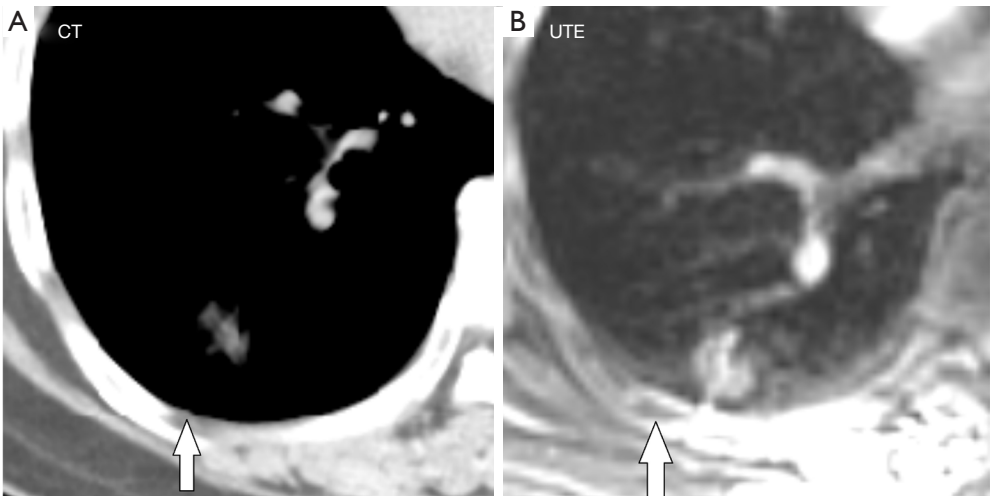

Figure 5 Detection of pleural indentations by UTE and CT. (A) No abnormal signal in the adjacent pleura on CT. (B) UTE sequence showed linear hyperintensity in the adjacent pleura of lesion. The arrow shows the pleural indentations. CT, computed tomography; UTE, ultrashort time of echo.

Table 4 Differentiation of malignant tumors by internal mixed signals of CT and UTE nodules

Project	Malignant neoplasm detected by CT	Malignant neoplasm detected by UTE	χ^2 value	P value
Number of patients	7	13	4.1	0.042
AUC	0.719	0.906		
95% CI	0.495–0.884	0.711–0.987		

CT, computed tomography; UTE, ultrashort time of echo; AUC, area under the curve; CI, concordance index.

is to use the ultrashort TE value (0.032 ms) to rapidly acquire MR signals of the short T2 components of matter before they decay rapidly to zero. If they decay, they are incomparable to conventional MRI scans. This means that UTE sequences can achieve better imaging results, representing a major breakthrough in the field of medical imaging, and their widespread application has important clinical significance. For example, when Ohno *et al.* (8) investigated the UTE sequencing technique and compared it with thin-layer conventional dose CT scans, their lung nodule detection rate of the latter was 92%, while the detection rate of the UTE sequence was 91.5% (there was no statistical difference between them). In addition, UTE–MRI technology has been applied to the identification of pulmonary nodules. Ohno *et al.* (18) used it to capture pulmonary nodules in a recent study and concluded that UTE–MRI is comparable to low-dose CT scanning in terms of lung nodule imaging. According to research by Delacoste *et al.* (19), the size of lung nodules can also be determined using UTE–MRI. In this regard, UTE–MRI results are comparable to CT results. It is clear that UTE–MRI technology has considerable potential for clinical applications involving the identification of pulmonary nodules and the determination of nodule size.

The results of the present study indicated that compared with CT scanning detection rate (97.8%), the detection rate of UTE–MRI sequencing for the total number of >4-mm nodules in the lung was 97.5%. One of the nodules did not appear in the UTE–MRI images, and its density in the CT scans was found to be light, with a CT value of around −850 Hu. In terms of the detection of lobulations, the image quality of UTE–MRI sequencing was consistent with that of CT scanning, which was in line with the results of previous studies (15). The image quality of CT imaging was higher than that of UTE–MRI in terms of the detection of spinous protuberances, with a statistically significant difference. The main reasons for this were likely the small size of the lesions, their low

edge density and their positioning in the basal segment of the lower lobe, close to the mediastinum, meaning they were susceptible to interference from heartbeats and respiratory motion artefacts. The secondary reason was likely the different respiratory status of the patients when performing the two examinations (CT is end-inspiratory imaging and UTE is free-end-expiratory imaging). Previous research has demonstrated that acquiring images at the end of exhalation and inhalation has an effect on the fine structure of nodules, especially powdered-glass nodules (compared with solid nodules), meaning there are likely to be inconsistencies among them. Given its use of respiratory gating, UTE–MRI is more convenient for patients who cannot hold their breath or for newborns (20). Furthermore, a self-navigating three-dimensional (3D) image-based MRI lung imaging technique has been established that enables motion-robust high-resolution 3D free-breathing lung MRI, demonstrating feasibility in patients with irregular breathing patterns (21).

The signal within a nodule in a UTE image is frequently more perplexing than in CT imaging, where it appears as a more homogeneous isointensity or as slightly hypointense. In this study, the number of cases of confounding nodules in the UTE–MRI method was higher than that in CT imaging, with a statistically significant difference. Furthermore, the probability of malignant tumours in the confounding nodules was significantly higher than that in the homogeneous nodules. This was primarily due to the higher soft-tissue resolution of the UTE–MRI technique, which is also more sensitive than CT to the presence of haemorrhaging, necrosis, mucus degeneration and fibrous components within lesions: factors that are more often seen in malignant tumours. Thus, the internal confounding nodules in UTE–MRI indicated that the technique is conducive to the accurate evaluation of the nature of nodules and that it provides a possibility for future evaluations of the efficacy of the early treatment of tumours.

The UTE–MRI technique demonstrated a slightly higher detection rate than that of CT imaging in terms of pleural indentation. Previous research discovered that the main cause of pleural indentation formation is intra-tumour scarring, which is related to visceral pleural indentation caused by tumour-induced pulmonary atelectasis (22). In the present study, the detection of pleural indentation in UTE–MRI was higher than that in CT imaging, mainly because the former was more sensitive than the latter to the signal display of water. Xiao *et al.* (16) confirmed one component of pleural indentation areas to be water, and that mild pleural indentation is poorly displayed in CT images.

The present study had some limitations. First, while the two imaging methods were compared, they were not compared with the pathological results, which may have led to some false positives. In the future, the number of patients with pulmonary nodules will need to be increased to study the presentation of various signs of lesions. Second, a number of patients with poor respiratory cooperation and poor image quality were excluded. Third, nodules of <4 mm in diameter were not included in this study; in the future, the scope of the research should be expanded to include more nodules. Finally, ground-glass nodules were not summarised separately, meaning the pleural retractions detected via UTE–MRI could have been false positives. Since this study imaged known nodules using a focused MRI approach, the nodule detection rate and the scan duration rate required in high-resolution UTE sequencing to cover the whole of the lungs was not clear, and further trials are needed to explore these factors.

Conclusions

The MRI technique has considerable potential for the identification of pulmonary nodules. The results of this study demonstrated that 3-T UTE–MRI has a high detection rate for pulmonary nodules >4 mm, similar to that of conventional CT imaging. The UTE technique is characterised by a TE that can be reduced to the microsecond level and is particularly suitable for the MRI of lung tissue with short T2 components and inhomogeneous magnetic fields. The method can be used for radiation-free lung cancer screening and follow-up examinations to reduce/eliminate both repeat CT examinations and radiation damage.

Acknowledgments

We wish to thank the timely help given by Tom Stimfield in language editing.

Funding: This study received funding from the Instructive Project of Xiamen Science and Technology Bureau in 2020 (No. 3502Z20209059).

Footnote

Reporting Checklist: The authors have completed the STARD reporting checklist. Available at https://qims.amegroups.com/article/view/10.21037/qims-22-118/rc

Conflicts of Interest: All authors have completed the ICMJE

uniform disclosure form (available at https://qims.amegroups.com/article/view/10.21037/qims-22-118/coif). The authors have no conflicts of interest to declare.

Ethical Statement: The authors are accountable for all aspects of the work in ensuring that any questions related to the accuracy or integrity of any part of the work were appropriately investigated and resolved. This study was conducted in accordance with the Declaration of Helsinki (as revised in 2013) and approved by the ethics committee of Fudan University Zhongshan Hospital Xiamen Branch. All patients signed an informed consent form prior to the examination.

References

1. Bray F, Ferlay J, Soerjomataram I, Siegel RL, Torre LA, Jemal A. Global cancer statistics 2018: GLOBOCAN estimates of incidence and mortality worldwide for 36 cancers in 185 countries. CA Cancer J Clin 2018;68:394-424.
2. Raghavan D, Wheeler M, Doege D, Doty JD 2nd, Levy H, Dungan KA, Davis LM, Robinson JM, Kim ES, Mileham KF, Oliver J, Carrizosa D. Initial Results from Mobile Low-Dose Computerized Tomographic Lung Cancer Screening Unit: Improved Outcomes for Underserved Populations. Oncologist 2020;25:e777-81.
3. Bianconi F, Fravolini ML, Pizzoli S, Palumbo I, Minestrini M, Rondini M, Nuvoli S, Spanu A, Palumbo B. Comparative evaluation of conventional and deep learning methods for semi-automated segmentation of pulmonary nodules on CT. Quant Imaging Med Surg 2021;11:3286-305.
4. Brenner DJ. Radiation risks potentially associated with low-dose CT screening of adult smokers for lung cancer. Radiology 2004;231:440-5.
5. Guneyli S, Tor M, Hassoy H, Aygun MS, Altinmakas E, Dik Altintas S, Savas R. Spin-echo and diffusion-weighted MRI in differentiation between progressive massive fibrosis and lung cancer. Diagn Interv Radiol 2021;27:469-75.
6. Xia Y, Guan Y, Liu SY, Fan L, Li B. Preliminary application of ultra short echo time (UTE) lung MR imaging in chronic obstructive pulmonary disease. J Clin Radiol 2018;37:401-5.
7. Burris NS, Johnson KM, Larson PE, Hope MD, Nagle SK, Behr SC, Hope TA. Detection of Small Pulmonary Nodules with Ultrashort Echo Time Sequences in Oncology Patients by Using a PET/MR System. Radiology 2016;278:239-46.
8. Ohno Y, Koyama H, Yoshikawa T, Seki S, Takenaka D, Yui M, Lu A, Miyazaki M, Sugimura K. Pulmonary high-resolution ultrashort TE MR imaging: Comparison with thin-section standard- and low-dose computed tomography for the assessment of pulmonary parenchyma diseases. J Magn Reson Imaging 2016;43:512-32.
9. Wielpütz MO, Lee HY, Koyama H, Yoshikawa T, Seki S, Kishida Y, Sakai Y, Kauczor HU, Sugimura K, Ohno Y. Morphologic Characterization of Pulmonary Nodules With Ultrashort TE MRI at 3T. AJR Am J Roentgenol 2018;210:1216-25.
10. Dournes G, Grodzki D, Macey J, Girodet PO, Fayon M, Chateil JF, Montaudon M, Berger P, Laurent F. Quiet Submillimeter MR Imaging of the Lung Is Feasible with a PETRA Sequence at 1.5 T. Radiology 2015;276:258-65.
11. Liu DL, Ma DQ, Chen G. The value of CT lobulation in imaging diagnosis of solitary pulmonary nodules. Chin J Radiol 2007;41:487-9.
12. Zwirewich CV, Vedal S, Miller RR, Müller NL. Solitary pulmonary nodule: high-resolution CT and radiologic-pathologic correlation. Radiology 1991;179:469-76.
13. Aoki T, Tomoda Y, Watanabe H, Nakata H, Kasai T, Hashimoto H, Kodate M, Osaki T, Yasumoto K. Peripheral lung adenocarcinoma: correlation of thin-section CT findings with histologic prognostic factors and survival. Radiology 2001;220:803-9.
14. Cui Y, Ma DQ, Yang J. Diagnostic value of pleural indentation in pulmonary nodules: a met analysis. Journal of Capital Medical University 2007;28:709-12.
15. Wielpütz MO, Lee HY, Koyama H, Yoshikawa T, Seki S, Kishida Y, Sakai Y, Kauczor HU, Sugimura K, Ohno Y. Morphologic Characterization of Pulmonary Nodules With Ultrashort TE MRI at 3T. AJR Am J Roentgenol 2018;210:1216-25.
16. Xiao XS, Wu HW, Li HM, Liu SY, Li CZ. CT and MRI Manifestations of Pleural Indentation in Peripheral Lung

Cancer: A Comparison with Pathological Findings. J Clin Radiol 2002;21:344-7.
17. Cieszanowski A, Lisowska A, Dabrowska M, Korczynski P, Zukowska M, Grudzinski IP, Pacho R, Rowinski O, Krenke R. MR Imaging of Pulmonary Nodules: Detection Rate and Accuracy of Size Estimation in Comparison to Computed Tomography. PLoS One 2016;11:e0156272.
18. Ohno Y, Takenaka D, Yoshikawa T, Yui M, Koyama H, Yamamoto K, Hamabuchi N, Shigemura C, Watanabe A, Ueda T, Ikeda H, Hattori H, Murayama K, Toyama H. Efficacy of Ultrashort Echo Time Pulmonary MRI for Lung Nodule Detection and Lung-RADS Classification. Radiology 2022;302:697-706.
19. Delacoste J, Dunet V, Dournes G, Lovis A, Rohner C, Elandoy C, Simons J, Long O, Piccini D, Stuber M, Prior JO, Nicod L, Beigelman-Aubry C. MR Volumetry of Lung Nodules: A Pilot Study. Front Med (Lausanne) 2019;6:18.
20. Jiang W, Ong F, Johnson KM, Nagle SK, Hope TA, Lustig M, Larson PEZ. Motion robust high resolution 3D free-breathing pulmonary MRI using dynamic 3D image self-navigator. Magn Reson Med 2018;79:2954-67.
21. Javed A, Ramasawmy R, O'Brien K, Mancini C, Su P, Majeed W, Benkert T, Bhat H, Suffredini AF, Malayeri A, Campbell-Washburn AE. Erratum to: Self-gated 3D stack-of-spirals UTE pulmonary imaging at 0.55 T (Magn Reson Med 2022;87:1784-1798). Magn Reson Med 2022;88:2326-7.
22. Wu HW, Xiao XS, Liu SY, Li HM, Li CZ, Liu HM. Intratumoral basis and related influencing factors of pleural indentation in peripheral lung cancer. Chin J Radiol 2001;10:11-5.

Cite this article as: Wang F, Lin X, Lin C, Huang G, Li M, Zhu L. Ability of three-dimensional 3-Tesla ultrashort echo time magnetic resonance imaging to display the morphological characteristics of pulmonary nodules: a sensitivity analysis. Quant Imaging Med Surg 2023;13(3):1792-1801. doi: 10.21037/qims-22-118

